Aeolian Research 20 (2016) 45–58

Contents lists available at ScienceDirect

Aeolian Research

journal homepage: www.elsevier.com/locate/aeolia

Threshold wind velocity dynamics as a driver of aeolian sediment mass flux

Nicholas P. Webb [a,*], Magda S. Galloza [a], Ted M. Zobeck [b], Jeffrey E. Herrick [a]

[a] USDA-ARS Jornada Experimental Range, MSC 3 JER, NMSU, Box 30003, Las Cruces, NM 88003, USA
[b] USDA-ARS Wind Erosion and Water Conservation Research Unit, 3810 4th Street, Lubbock, TX 79415, USA

ARTICLE INFO

Article history:
Received 12 June 2015
Revised 7 November 2015
Accepted 9 November 2015

Keywords:
Wind erosion
Dust
Erodibility
Transport
Sediment flux
Supply limitation

ABSTRACT

Horizontal (saltation) mass flux is a key driver of aeolian dust emission. Estimates of the horizontal mass flux underpin assessments of the global dust budget and influence our understanding of the dust cycle and its interactions. Current equations for predicting horizontal mass flux are based on limited field data and are constrained to representing transport-limited equilibrium saltation, driven by the wind momentum flux in excess of an entrainment threshold. This can result in large overestimation of the sediment mass flux. Here we compare measurements of the soil entrainment threshold, horizontal mass flux, and their temporal variability for five undisturbed dryland soils to explore the role of threshold in controlling the magnitude of mass flux. Average and median entrainment threshold showed relatively small variability among sites and relatively small variability between seasons, despite significant differences in soil surface conditions. Physical and biological soil crusts had little effect on the threshold value, and threshold appeared to play a minor role in determining the magnitude of sediment transport. Our results suggest that horizontal mass flux was controlled more by the supply limitation and abrasion efficiency of saltators present as loose erodible material or originating from neighboring soil sources. The omission of sediment supply and explicit representation of saltation bombardment from horizontal flux equations is inconsistent with the process representation in dust emission schemes and contributes to uncertainty in model predictions. This uncertainty can be reduced by developing greater process fidelity in models to predict horizontal mass flux under both supply- and transport-limited conditions.

Published by Elsevier B.V.

1. Introduction

A fundamental challenge in aeolian research is to accurately predict the horizontal (saltation) mass flux for varying soils and surface conditions. In most dust emission models the horizontal mass flux (Q) is calculated independently of the vertical (dust) flux, following physically based equations that are parameterized to represent measurements of sand transport rates (e.g., Bagnold, 1937; Kawamura, 1951; Owen, 1964; Lettau and Lettau, 1978; Shao et al., 1993). In general, these equations predict that Q scales with the third power of the wind shear velocity (u_*, m s^{-1}) and the proportion of shear velocity that is in excess of an entrainment shear velocity threshold (u_{*_t}). For example (after Owen, 1964):

$$Q = C\frac{\rho_a}{g}u_*^3\left(1-\frac{u_{*_t}^2}{u_*^2}\right) \quad (u_* \geqslant u_{*_t}) = 0 \quad (u_* < u_{*_t}), \tag{1}$$

where Q has the units of kg m^{-1} s^{-1}, ρ_a is the air density (kg m^{-3}) and g is the acceleration of gravity (m s^{-2}). C is a dimensionless fitting parameter.

The equations typically follow Owen's hypotheses that (1) the saltation layer behaves as an aerodynamic roughness whose height is proportional to the thickness of the layer, and (2) the concentration of particles within the saltation layer exists in a steady state and is thus in equilibrium with the wind momentum flux incident on the bed (Owen, 1964). It has been shown that feedback between the saltation layer and aerodynamic roughness produces a convergence of velocity profiles around a focal point whose height is determined by the flux density, grain trajectories and their vertical distribution (Bagnold, 1941; Sherman, 1992; Duran et al., 2011; Jenkins and Valance, 2014). However, the assumption of equilibrium transport scaling with u_*^3 and driven solely by $u_* > u_{*_t}$ is often not consistent with measurements under field conditions (Namikas and Sherman, 1995; Sherman and Farrell, 2008; Sherman and Li, 2012; Sherman et al., 2013; Rotnicka, 2013). This is a recognized source of uncertainty in transport predictions.

* Corresponding author. Tel.: +1 575 646 3584; fax: +1 575 646 5889.
E-mail address: nwebb@nmsu.edu (N.P. Webb).

http://dx.doi.org/10.1016/j.aeolia.2015.11.006
1875-9637/Published by Elsevier B.V.

Recently progress has been made to numerically resolve saltation mechanics (e.g., Werner, 1990; Creyssels et al., 2009; Kok and Renno, 2009). This work has provided insights into the feedbacks between the saltation layer and wind velocity profile over erodible and rigid beds (Duran et al., 2012; Charru et al., 2013; Jenkins and Valance, 2014). It has also been shown that the scaling of Q with u_* varies with bed hardness (Ho et al., 2011; Jenkins and Valance, 2014) and moisture content (Rotnicka, 2013), and that these surface conditions also moderate the occurrence of equilibrium or non-equilibrium saltation (McKenna Neuman and Scott, 1998; Wiggs et al., 2004). Observations suggest that saltator availability, bed hardness and saltation bombardment may have a greater effect on horizontal mass flux than u_{*_t} in supply-limited systems (Gillette and Chen, 2001; Gillies et al., 2014). This appears to be consistent across the major global dust source areas (e.g., Chappell et al., 2008), but the physical mechanisms have not been fully resolved with experimental data.

Representing the effects of sediment supply limitation, bed hardness, and saltation bombardment on horizontal mass flux remains an ongoing challenge (Shao, 2008). One approach, described by Bagnold (1941) in formulating the transport equation, is to account for bed characteristics and sediment supply by modifying C in Eq. (1) (e.g., Gillette and Chen, 2001). Modifying the flux equation exponent and proportionality factor may also provide a solution for representing effects of bed hardness (Ho et al., 2011; Jenkins and Valance, 2014). However, a generalizable approach for accurately predicting Q across soil types and surface conditions has so far been elusive. While saltation bombardment and surface cohesion are explicitly represented in some dust emission schemes (e.g., Shao et al., 2011; Kok et al., 2014), approaches do not yet determine Q as a function of these processes and for supply-limited systems where the ratio u_{*_t}/u_* (Eq. (1)) may not be a reliable predictor of sediment transport.

Accurately determining the soil entrainment threshold remains key to establishing the controls on timing and magnitude of horizontal mass flux in both transport- and supply-limited systems. Considerable attention has been given to determining the entrainment threshold for different soils (e.g., Gillette et al., 1980) and the effects of soil disturbance (e.g., Belnap et al., 2007). The majority of this work has been conducted using laboratory and field wind tunnel experimentation, as reviewed by Webb and Strong (2011). This work has provided insights into the potential variability in the entrainment threshold through its response to changing environmental conditions. Nonetheless, our understanding as formalized in sediment flux equations derives almost exclusively from studies that consider the role of threshold under transport-limiting conditions (e.g., Bagnold, 1937; Kawamura, 1951; Owen, 1964; Lettau and Lettau, 1978; Shao et al., 1993).

Challenges arise when translating the findings of wind tunnel studies of threshold to understand sediment flux dynamics in supply-limited settings. These include (1) unless repeated, the studies often provide snapshots of the entrainment threshold at a specific point in time, perhaps relating only to the condition of the soil surface during experimental measurements (typically lasting < 30 min) (e.g., Gillette et al., 1980), and (2) both results and interpretation are strongly influenced by the measurement scale of wind tunnels, which do not capture spatial variability in sediment supply or produce large turbulence structures that can drive sediment transport (Sherman and Farrell, 2008). The implications are that little remains known about threshold dynamics that influence the timing and magnitude of sediment transport (Barchyn and Hugenholtz, 2012). Measurements from wind tunnels, that have formed the basis of our understanding, may not always be representative of the processes driving Q in supply-limited landscapes where sparse available saltators on the soil surface or originating from neighboring surfaces (e.g., source bordering dunes) may be responsible for driving the sediment transport process (Macpherson et al., 2008). Understanding threshold dynamics at the field scale is needed as a basis for evaluating controls on horizontal mass flux and developing greater process fidelity in aeolian sediment transport models.

This paper evaluates threshold wind velocity dynamics in undisturbed supply-limited dryland landscapes. The scope of the paper is to explore, based on field measurements and our understanding of process, possible factors driving variability in Q not explained by variability in entrainment threshold. The paper objectives are to (1) evaluate the magnitude of horizontal mass flux for five undisturbed dryland soils, (2) quantify temporal variability in the threshold wind speed (U_t) at which mass flux is initiated, and (3) describe the characteristics of threshold dynamics relative to other factors that may influence sediment transport. The research aims are addressed using data from the Chihuahuan Desert of southern New Mexico, USA. We compare and contrast soil entrainment thresholds and their temporal variability among sites to examine, within the limits of the data, the significance of threshold dynamics and the implications for wind erosion modeling.

2. Methods

2.1. Site description

Five field sites were established at the Jornada Experimental Range in southern New Mexico, USA, in April 2013 (Fig. 1). The sites were selected to represent the range of soil textures and surface conditions that frequently emit dust in the region (Floyd and Gill, 2011). They are located across five vegetation/soil complexes that are typical of the northern Chihuahuan Desert, as studied by Bergametti and Gillette (2010). Plant community composition in the study area varies with soils, elevation and landscape position. The historic plant communities at the sites are C_4 grasslands or mixed communities of warm-season grasses, shrubs and half-shrubs (McClaran and Van Devender, 1997).

Site 1 is located on sandy clay loam soil (US Department of Agriculture classification) within a crusted playa surrounded by tobosa grass (*Pleuraphis mutica* Buckley) and burrograss (*Scleropogon brevifolius* Phil.). The location has an exposed bare fetch ~100 m in length and ~40 m wide extending to the southwest from the site. Site 2 is located on a loam soil within a broad (~5 ha) open playa with mixed physical and biological (cyanobacteria, lichen) soil crusts. The site is surrounded by sparse patches of burrograss ~50 m from the instrumentation. Site 3 is centered in a smaller (~2 ha), predominantly bare, playa with sandy clay loam soil surrounded by a sand ridge ~2 m high covered with dropseed (*Sporobolus* R. Br.) and creosote (*Larrea tridentata* DC). Site 4 is located on a sandy loam soil with sparse mixed cover dominated by honey mesquite (*Prosopis glandulosa* Torr.) and purple threeawn (*Aristida purpurea* Nutt.). Site 5 is also located on a sandy loam soil, supporting a diverse community including honey mesquite, black grama (*Bouteloua eriopoda* Torr.) and dropseed.

The mean annual precipitation (1915–2014) for the study area is 250 mm (coefficient of variation 35%), with 60% falling in the summer months from June through September. The mean annual maximum and minimum temperatures range from 25 °C to 5 °C (Wainright, 2006). Land surrounding the study sites is periodically grazed by cattle.

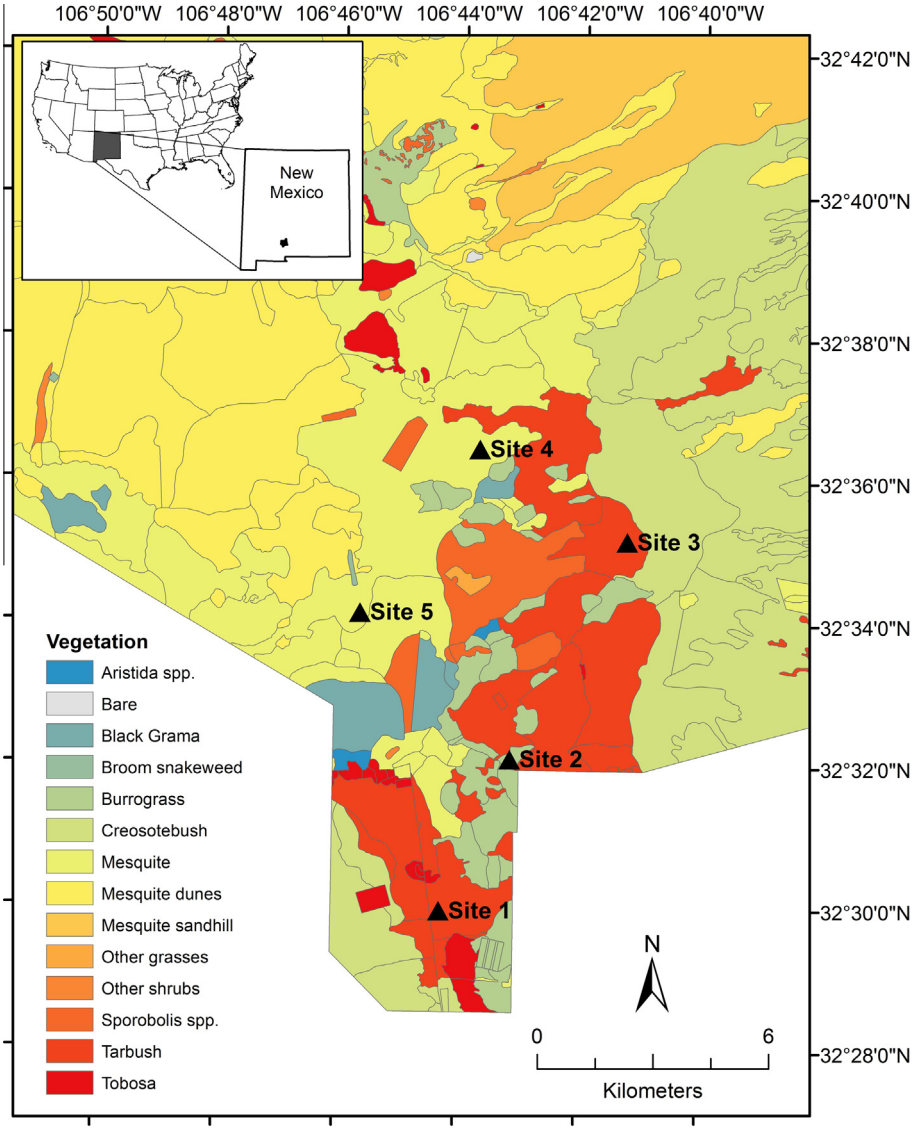

Fig. 1. Study area map showing the location of the Jornada Experimental Range (JER) in New Mexico, USA, and the five study site locations within the JER. Dominant vegetation types are shown for the study area as context for those in the Chihuahuan Desert, which extends toward the southeast into Mexico.

2.2. Instrumentation

The five study sites were instrumented to measure horizontal sediment mass flux, wind speed profiles and threshold wind speeds for soil entrainment (Fig. 2). A 5.0 m meteorological tower was centrally located at each site, on which were mounted RM Young 3101 cup anemometers at heights of 0.7 m, 1.4 m and 2.4 m above ground level, and one RM Young 3002 anemometer and wind vane at 4.8 m height. A tipping bucket rain gauge (model TE-525) was located adjacent to each tower at 1.5 m above ground level.

A Wenglor optical gate sensor (model YH03PCT08, 30 mm fork width), used to measure saltation particle counts, was mounted on a wind vane at 0.05 m above ground level to the southwest of each tower. The instrument movement was restricted such that saltation counts were sampled between 180° and 270°, corresponding with the dominant erosive wind direction (Gillette et al., 2006). We assume that measures of the entrainment threshold from the Wenglors provide a good approximation of threshold for the sites, noting that these estimates may be lower than those made by Sensit saltation impact sensors (Massey, 2013). Each Wenglor was cleaned one to two times per week to remove dust that can block the sensor (Barchyn et al., 2014). Data from all instruments were sampled at 1 Hz and averages, maximums and totals were logged every 1 min on a Campbell Scientific CR1000 data logger. Data for this study were collected from 18 May, 2013 to 15 May, 2014.

The horizontal sediment mass flux was measured using Modified Wilson and Cooke (MWAC) samplers with inlet 0.4715 cm^2 (after Goossens et al., 2000). Two masts, each equipped with four MWAC samplers (0.1 m, 0.25 m, 0.5 m and 0.85 m above ground level) and able to rotate 360° to orient into the wind were located to the northwest and southwest of the meteorological tower. Each study site was enclosed with a 20 × 20 m wire fence to exclude livestock.

2.3. Field data collection and laboratory analysis

The fractional ground cover (including vegetation, litter, rock, physical and cyanobacterial crusts and loose erodible material) and vegetation canopy height were calculated from data collected along three 100 m transects at each site at the time of site establishment. Soil crust hardness to point of rupture was measured

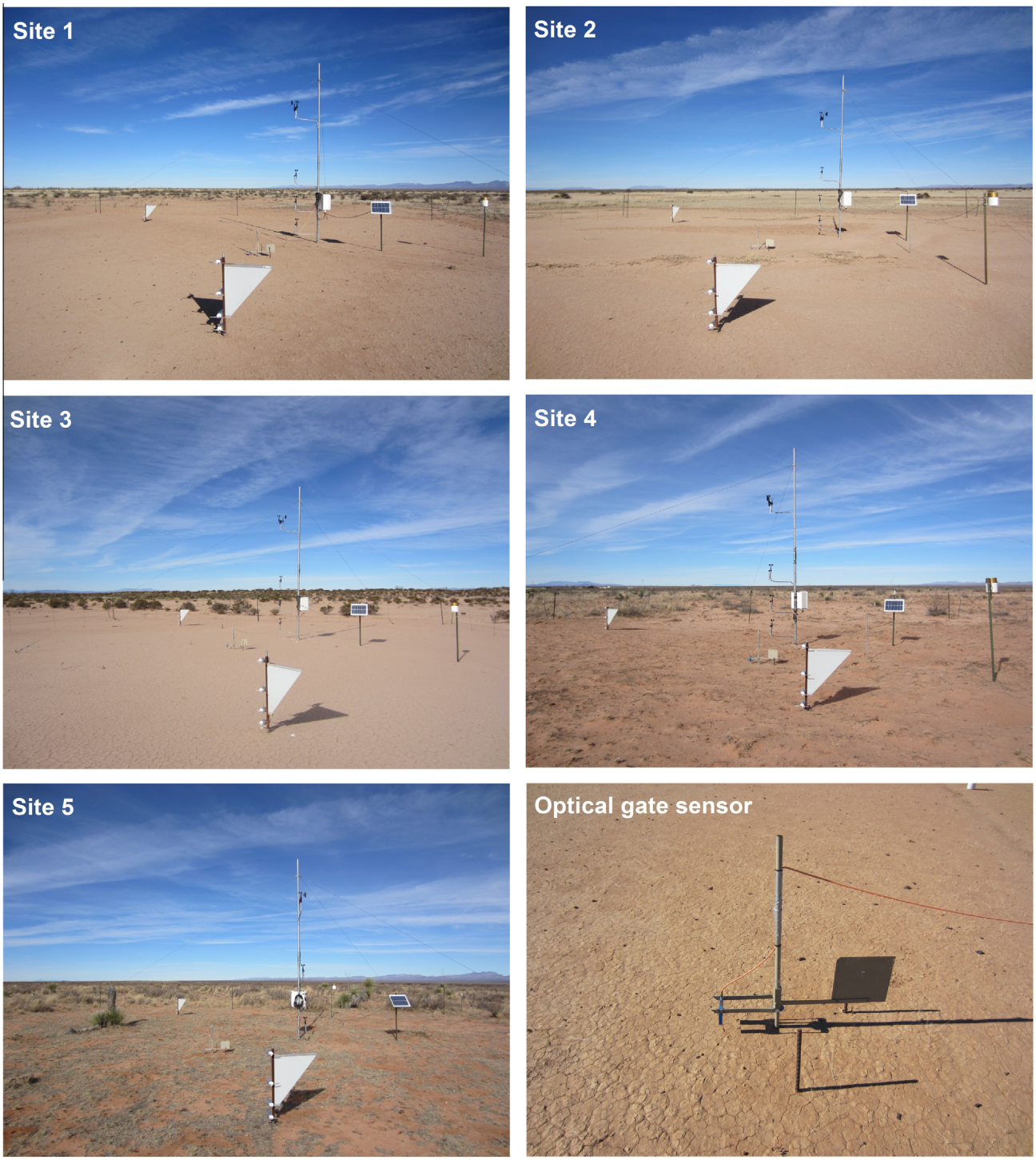

Fig. 2. Photographs of the five study sites showing meteorological towers, two MWAC sediment samplers and close-up view of a Wenglor optical gate sensor mounted on a wind vane. Stakes either side of the wind vane restrict the Wenglor rotation so that it samples within the range 180°–270°. Photographs were taken from the south, facing north.

using a handheld penetrometer (Zobeck et al., 2003; QA Supplies, model FT011) with a flat 10 mm diameter foot applied at 45° to the surface. Line-point intercept sampling with a point spacing of 1.0 m was used for data collection (Herrick et al., 2005). Transects were placed in a spoke pattern, intersecting at the center of each site and spaced at 60° intervals. After sampling, all plots were cleared of vegetation to the surface and were maintained in a bare condition for the duration of the study. This treatment ensured that the soil threshold wind speeds and horizontal mass fluxes could be evaluated without the complicating effects of vegetation (Webb et al., 2014). Surface crusts were disturbed during vegetation clearing but were observed to recover with the next rainfall event. After site establishment clearing was only conducted during the summer monsoon period (July–August), so we expect the disturbance had only a short-term effect on the site erodibility.

Vegetation cover was stable at Sites 1, 2 and 3 for which vegetation was sparse and naturally absent within the study plots. At Sites 4 and 5 the vegetation cover outside the cleared study sites was observed to increase over summer as the grasses and deciduous mesquite shrubs responded rainfall, resulting in some increase in the aerodynamic roughness (z_0; Section 2.4). Repeat measurements were not made of the soil properties as this would have disturbed the soil surface. Repeat photography of the sites was therefore used to help interpret the soil erodibility changes over time.

At each site, 10 soil samples (250 g each) were collected of the uppermost 0.01 m from random locations for analysis of the particle size distribution, organic carbon (C), nitrogen (N), and carbonate ($CaCO_3$) contents. High-resolution particle size analyses (PSAs) of the soils were conducted using a Beckman Coulter LS 13 320 MW laser diffraction particle size analyzer. Soils were then grouped into USDA textural classes for comparison (Soil Survey Division Staff, 1993). Five composited sub-samples from each site were analyzed in both dry (minimally dispersed at atmospheric pressure) and wet (chemically dispersed with sodium hexametaphosphate) conditions following the methods of Zobeck (2004). PSAs were run for each of the dry and dispersed subsamples and the data were then averaged to provide an estimate of the minimally and fully dispersed PSD over 255 size classes for each site.

Samples were analyzed for organic C and N contents using an Elementar Vario Max C–N analyzer (Elementar Americas Inc., Mt Laurel, New Jersey) following Zobeck et al. (2013). Analyses of the soil $CaCO_3$ contents were conducted following the volumetric inorganic carbon determination method of Wagner et al. (1998). Five sub-samples were analyzed for each site and the average and standard deviation (SD) of the C, N and $CaCO_3$ contents were then calculated for each site.

Sediment was collected from the MWAC samplers at each field site at a monthly frequency. Sample masses were determined after rinsing with distilled water and drying at 65 °C overnight. Some samples from Sites 4 and 5 were contaminated over summer 2013 due to insects building mud nests in the MWAC inlet tubes. These data were removed from the analysis.

2.4. Data analysis

Wind speed data for each site (2.4 m above ground level) were summarized to evaluate the number of hours and probabilities of potentially erosive winds ($\geqslant 5$ m s^{-1}) within each sediment sampling period. Total rainfall (mm) was calculated for the corresponding sampling periods. Wind speed profile data were then used to estimate the aerodynamic roughness height (z_0) for each site following the Prandtl-von Kármán logarithmic velocity profile law:

$$\frac{U_z}{u_*} = \frac{1}{k}\ln\left(\frac{z}{z_0}\right), \tag{2}$$

where U_z is the wind speed (m s^{-1}) at height z (m), u_* is the wind shear velocity (m s^{-1}) and k is von Kármán's constant (0.4). In the absence of air temperature profiles that could be used to establish atmospheric stability, the 1 min wind speed data were resampled to 15 min averages. Values of z_0 were then established for periods without sediment transport through extrapolations to the y-axis intercept of the plot of wind speed against the logarithm of the anemometer heights above ground level, enabling regression analysis of the form:

$$y = mx + c, \tag{3}$$

where $u_* = km$ and $z_0 = \exp(-c/m)$, following Wiggs et al. (1996) and Zobeck et al. (2003). Correlation coefficients of the regression were analyzed and data with $R^2 < 0.97$, wind speed $\leqslant 2$ m s^{-1} (0.7 m height) and values of $z_0 < 1 \times 10^{-5}$ and $z_0 > 0.1$ m were removed (Marticorena et al., 2006). Data were also filtered for the directional range $180° < U < 270°$, consistent with the Wenglor sensing range. The data selection ensured that the wind speed profiles were not adversely affected by atmospheric instability and were above the minimum sensitivity of the anemometers (0.5 m s^{-1}). Two anemometers at Site 4 reported spurious values for much of the study period. We therefore do not report z_0 values for that site. We expect, given the soil and vegetation conditions at the site, that z_0 for Site 4 would be similar to that for Site 5. However, despite data filtering for quality assurance, we were unable to establish significant differences in z_0 among the sites due to the large uncertainty in the estimates. For this reason we did not standardize the data for the aerodynamic roughness by calculating u_{*t}, and report wind speed thresholds (U_t) instead (e.g., Stout and Arimoto, 2010; Barchyn and Hugenholtz, 2011).

Threshold wind speeds (U_t) were established following the instantaneous threshold method (Barchyn and Hugenholtz, 2011). Here U_t is the wind speed (2.4 m above ground level) at which soil entrainment is initiated, producing a Wenglor pulse count of 10 grains per minute. Summary statistics (minimum, maximum, mean, median and quantiles) for U_t were calculated for each site and for the data categorized within each site by season.

Kernel density estimates of U_t were developed to visualize variability in the wind speed threshold among sites and between seasons (Barchyn and Hugenholtz, 2012). Briefly, each value of U_t in the measured range (x_i, $i = 1,...n$) was assigned a normal distribution, centered on the value of U_t and having a standard deviation designated h (0.03–0.06 m s^{-1}). The normal distributions were then summed for each site and for each season to provide the kernel density estimates given by:

$$\widehat{f}(x,h) = \frac{1}{nh}\sum_{i=1}^{n}\phi\left(\frac{x-x_i}{h}\right), \tag{4}$$

where $\widehat{f}(x,h)$ is the height of the curve at x, and ϕ is the standard normal density (Thomson, 2006). The analysis was conducted using Microsoft Excel with an Analytical Methods Committee (AMC) Software add-in (Thomson, 2006).

Horizontal sediment mass flux was calculated from sediment masses collected with the MWAC samplers. Exponential functions were fitted using nonlinear least squares regression to data, normalized by the MWAC inlet area (0.4715 cm^2), from each MWAC mast where sediment profiles were available from all four samplers:

$$q(z) = ce^{(az^2+bz)}, \tag{5}$$

where a, b and c are coefficients of the fitted function and z is the height above the surface (in cm). The fit provided an average R^2 of 0.99 across all of the profiles for the sites. Total (integrated) horizontal sediment mass fluxes (Q) were calculated by integrating the exponential functions from the surface (0 cm) to 100 cm height and dividing by the sampling period:

$$Q = \int_0^{100} q(z)dz, \tag{6}$$

where Q was expressed with units of g cm^{-1} month^{-1}. The magnitude and variability in the measured Q and U_t were then interpreted in the context of the site soil characteristics and seasonal patterns of wind erosivity and rainfall.

3. Results and discussion

3.1. Soil characteristics

The five study sites had a range of soil texture, varying from sandy loam with 11% clay (Site 5), to sandy clay loam with 25% clay (Site 3) (Table 1). Differences in soil texture among sites contributed to the observed differences in surface characteristics. The finer-textured Sites 1, 2 and 3 had complete cover of physical soil crusts, with some cyanobacterial crusts at Site 2, and a small fraction (<6%) of the bare soil surfaces covered with loose erodible material. Sites 4 and 5 have coarser soils (sandy loam) and during site establishment had large cover (>40%) of loose erodible sediment overlying patchy cyanobacterial soil crusts.

Site 2 had the hardest soil surface (3.38 kg cm^{-2} to rupture) while Sites 1 (1.69 kg cm^{-2}) and 3 (1.87 kg cm^{-2}) had similar crust hardness and Sites 4 and 5 had the weakest surface crusts (~0.5 kg cm^{-2}) (Table 1). At Sites 4 and 5, 90% of the penetrometer measurements were below the measurable range (<0.5 kg cm^{-2}), while at Sites 2 and 3, 39% and 36% of measurements were above the measurable hardness range (>5 kg cm^{-2}). Soil surface hardness is dynamic (Rice and McEwan, 2001) and we expect that, like vegetation cover, this characteristic responded to rainfall events.

Comparison of the minimally and fully dispersed soil PSDs demonstrates considerable aggregation in all five soils (Fig. 3 and Table 1). We interpret the minimally dispersed PSDs for Sites 4 and 5 as providing a good approximation of the soils *in situ*. In this field condition the soil PSDs are dominated by grains in the sand fraction (>100 μm) that may be available as saltators in the loose erodible material. The silt and clay fraction in the soils increased dramatically in the fully dispersed PSDs, suggesting that despite having a sandy surface texture these soils have potential to be dust emitters. The minimally dispersed PSDs for Sites 1, 2 and 3 do not represent well the condition of the soil observed in the field. The fine texture of the soils lends to the extensive physical soil crusting at these sites (Table 1).

Soil organic C and N contents were small at all sites (<1% C; <0.05% N). However, large variability was measured in the soil $CaCO_3$ contents (Table 1), which is attributable to pedogenic carbonate accumulation in the Jornada Basin soils. Variability in $CaCO_3$ contents of the surface soil among the sites has arisen as a consequence of bioturbation (Site 4) and differences in depth of wetting during petrocalcic horizon formation and subsequent erosion and deposition (Sites 2 and 3) (Monger, 2006). The presence of soil $CaCO_3$ at the sites was expected to influence the soil cohesiveness, potentially reducing U_t (Chepil, 1954).

3.2. Wind erosivity, aerodynamic roughness and rainfall

The frequency of potentially erosive winds was strongly seasonal, while the number hours with high wind speeds varied among the sites (Fig. 4a). Early summer 2013 (June and July) and spring 2014 (April and May) experienced the most erosive winds, with >100 h of wind speed $\geqslant$5 m s^{-1} (2.4 m above ground level) at Sites 1, 2, 3 and 5. Lower wind speeds were measured at Sites 4 and 5 in all months of the study period. Site locality with respect to the Doña Ana Mountains and Summerford Mountain, which obstruct the dominant south-westerly winds, likely influenced wind erosivity among sites. Vegetation cover in close proximity to the sites potentially also increased U_t and reduced sediment transport at Sites 4 and 5, relative to Sites 1, 2 and 3. Our entrainment threshold estimates must therefore be interpreted understanding that larger differences in U_t may exist between the

Table 1
Soil properties and surface characteristics at the five Chihuahuan Desert study sites, measured at the time of site establishment in April, 2013. Values are reported as a percentage (%) unless otherwise noted. Mean and standard deviation (SD) values are reported for the soil $CaCO_3$, organic carbon and nitrogen contents. Values for the soil surface characteristics are reported as percentage cover of the soil surface.

	Site 1	Site 2	Site 3	Site 4	Site 5
Soil properties (0–1 cm)					
Texture – Minimally dispersed					
Clay	16.25	19.08	5.09	1.84	0.27
Silt	37.41	44.66	14.87	7.02	3.28
Sand	46.34	36.26	81.04	91.13	95.55
Texture – Fully dispersed					
Clay	22.07	21.33	24.94	16.27	10.99
Silt	25.29	32.28	21.46	22.29	21.91
Sand	52.63	46.39	53.60	61.44	67.10
USDA texture class	Sandy clay loam	Loam	Sandy clay loam	Sandy loam	Sandy loam
Soil map unit component[a]	Stellar	Reagan	Reagan	Harrisburg	Bucklebar
$CaCO_3$ (SD)	0.13 (0.10)	9.09 (0.65)	18.27 (2.35)	4.02 (3.13)	0.01 (0.03)
Organic carbon (SD)	0.97 (0.12)	0.78 (0.15)	0.44 (0.06)	0.42 (0.39)	0.26 (0.05)
Nitrogen (SD)	0.04 (0.01)	0.037 (0.01)	0.019 (0.00)	0.05 (0.03)	0.03 (0.01)
Soil surface characteristics					
Physical crust	71.67	54.00	92.67	–	–
Cyanobacteria crust	–	28.67	–	34.67	23.67
Physical clay curls	–	11.00	–	–	–
Rock	1.00	–	1.00	2.67	–
Loose erodible material	4.00	2.00	6.00	46.33	42.67
Penetrometer resistance, kg cm^{-2} (SD)	1.69 (0.81)	3.38 (1.23)	1.87 (0.99)	0.54 (0.02)	0.50 (0.01)
Vegetation					
Canopy cover (%)	29.67	9.33	2.67	14.00	30.00
Mean canopy height (m)	0.13	0.07	0.41	0.19	0.41
Slope (%)	<1	<1	<1	<1	<1

[a] Soil Map Unit Components represent individual soils that occur within delineated Soil Map Unit polygons, as mapped by the U.S. Department of Agriculture (USDA) Natural Resources Conservation Service.

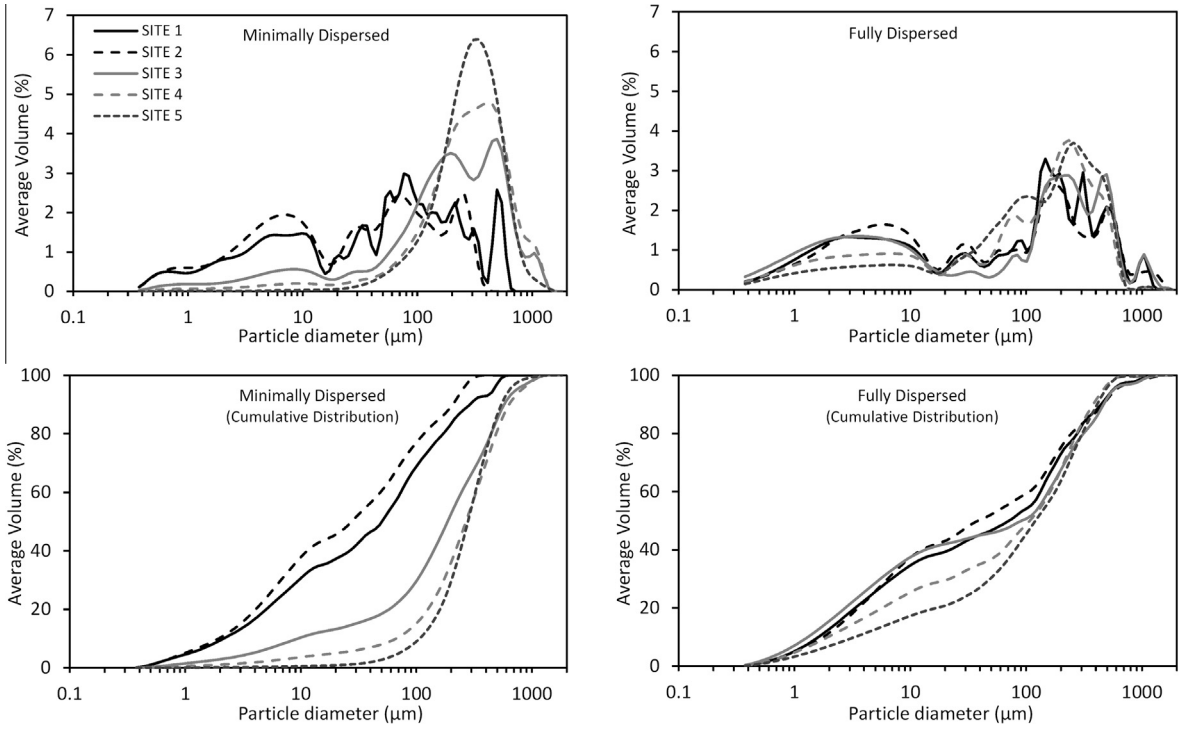

Fig. 3. Particle size distributions and cumulative particle size distributions for the five study soils, determined using a Coulter LS 13 320 particle size analyzer. Soils were analyzed in minimally and fully (chemically) dispersed conditions (see Section 2 for details).

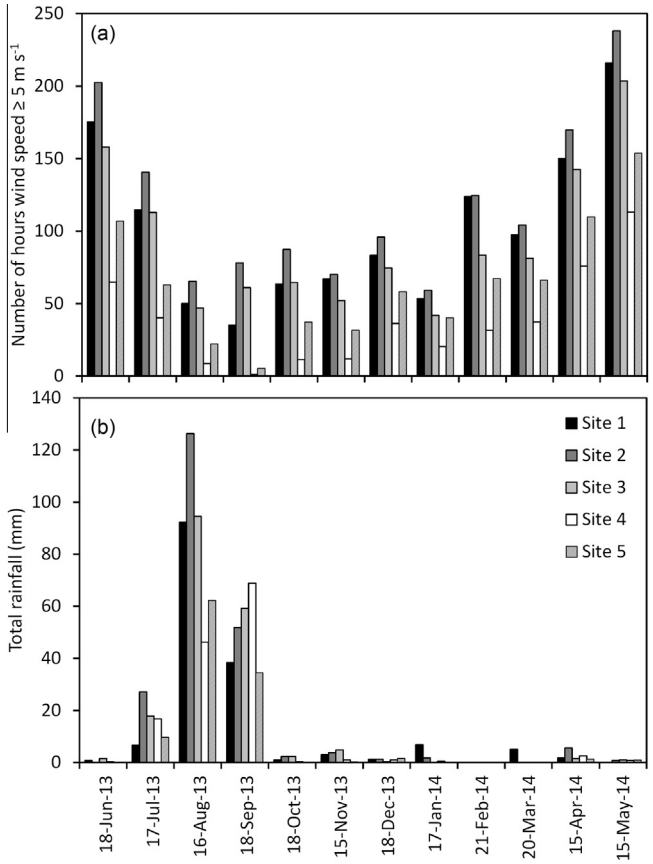

Fig. 4. (a) Mean monthly occurrence of wind speed $\geqslant 5\ m\ s^{-1}$ (measured at 2.4 m above ground level), and (b) total monthly precipitation for the five study sites. Note, months displayed correspond with the sediment sampling periods. Sampling was initiated on 18 May, 2013.

study soils if the roughness conditions were exactly the same for all sites. As the meteorological tower and optical gate sensor (for measuring U_t) were located at the center of the study sites, the measurements would not have been affected by sheltering due to vegetation but would have been affected by roughness in the fetch (100s of meters) upwind of the sites. Consistent with Bergametti and Gillette (2010), the seasonal wind speed pattern suggests that the study sites may experience strongly seasonal sediment mass flux, with a peak during spring and low during the summer and autumn.

The mean monthly aerodynamic roughness heights (z_0) were of a similar magnitude (Table 2) for Sites 1, 2 and 3, consistent with the soil surface conditions (Table 1). At all sites the coefficient of variation in z_0 was large, and up to two times the monthly mean value. At Sites 1, 2, and 3, z_0 was of the order 1 cm, with a seasonal pattern with maximum (~1.5 cm) during the winter months (December–February) and minimum through summer 2013. Values of mean z_0 were larger for Site 5, in the range 3–5 cm (Table 2). The larger z_0 values at this site were likely a function of the taller vegetation in the fetch surrounding the cleared exclosure (Table 1) and topography at the soil surface. Vegetation growth in response to summer rainfall is responsible for the peak in z_0 during autumn 2013. The roughness of the soil crusts at Sites 1, 2 and 3 was not observed to change significantly over the study period and likely had little effect on the changes in z_0 relative to the surrounding vegetation. While we observed soil crust cover change at Sites 4 and 5, these changes were also small relative to the soil topography and vegetation.

Rainfall during the study period was more strongly seasonal than wind speed (Fig. 4b). Between 110 mm (Site 5) and 220 mm (Site 2) rainfall was recorded across the sites for the study period. On average 93% of the rainfall at the sites occurred in the summer months (July, August and September).

Table 2
Summary of mean aerodynamic roughness height (z_0) and standard deviations (SD) for each sampling period. Sampling started on 18 May 2013 and data are based on 1 min average wind speed measurements resampled to 15 min averages. Note: data for Site 4 are not provided due to equipment failure (Section 2.4).

Sampling period end	Site 1		Site 2		Site 3		Site 5	
	Mean z_0 (cm)	SD	Mean z_0 (cm)	SD	Mean z_0 (cm)	SD	Mean z_0 (cm)	SD
06/18/2013	0.80	1.76	0.51	1.47	0.49	1.35	2.94	2.13
07/17/2013	0.67	1.62	0.51	1.44	0.39	1.24	2.13	2.05
08/16/2013	0.84	1.80	0.60	1.57	0.51	1.47	2.56	2.26
09/18/2013	1.32	2.32	0.97	2.08	0.81	1.80	4.04	2.78
10/18/2013	0.89	1.85	0.68	1.73	0.53	1.53	5.24	2.21
11/15/2013	0.73	1.55	0.62	1.62	0.61	1.59	4.94	2.51
12/18/2013	1.13	1.98	0.85	1.87	0.54	1.49	3.47	2.19
01/17/2014	1.26	1.97	0.81	1.80	0.61	1.63	3.09	2.11
02/21/2014	1.06	1.76	0.60	1.47	0.64	1.60	3.09	2.13
03/20/2014	0.99	1.81	0.64	1.56	0.46	1.32	2.92	2.05
04/15/2014	0.94	1.84	0.47	1.45	0.49	1.44	2.73	1.93

Table 3
Monthly average vertically integrated horizontal sediment mass flux (g cm^{-1} month^{-1}) to 1 m height above the soil surface for the five study sites. Sampling commenced on 18 May 2013. Values marked with * represent integrated flux from a single measured profile, while all other values represent an average horizontal sediment mass flux from the two MWAC mast profiles. Values marked with "-" indicate that insufficient samples were obtained from both MWAC profiles to calculate the integrated mass flux.

Sampling period end	Vertically integrated horizontal sediment mass flux (g^{-1} cm^{-1} month^{-1})				
	Site 1	Site 2	Site 3	Site 4	Site 5
06/18/2013	8.41	4.10*	19.96	108.61	29.72
07/17/2013	13.94	14.07	94.10	102.60	43.41
08/16/2013	28.34	36.38	287.05	56.79*	53.80
09/18/2013	12.42*	15.68	125.47	-	-
10/18/2013	19.18*	8.08	133.12	-	-
11/15/2013	10.13	5.23	-	64.38	-
12/18/2013	2.21*	3.24	41.26	43.87	-
01/17/2014	1.22	1.11	5.20	2.79	-
02/21/2014	-	1.99*	8.91	36.47	-
03/20/2014	9.70	4.59	53.75	65.50	3.43*
04/15/2014	4.98	5.63	47.57	57.86	3.69
05/15/2014	7.52	8.22	44.41	185.81	15.46

3.3. Horizontal sediment mass flux

Horizontal sediment mass flux varied by up to two orders of magnitude among sites and between sampling periods (Table 3). The largest sediment fluxes were recorded at Sites 3 (287.05 g cm^{-1} month^{-1}) and 4 (185.81 g cm^{-1} month^{-1}), while the smallest sediment fluxes were recorded at Sites 1 (1.11 g cm^{-1} month^{-1}) and 2 (1.12 g cm^{-1} month^{-1}). Intermediate sediment fluxes were recorded at Site 5, but of a similar magnitude to Sites 1 and 2. Larger sediment mass flux may have been recorded at Sites 4 and 5 if the vegetation cover and distribution in the fetch leading to the sites were more like that at Sites 1, 2 and 3; perhaps enabling the saltation cascade to develop closer toward equilibrium than could be achieved within the cleared 20 × 20 m study exclosures. As expected, the sediment mass flux close to the soil surface (0.1 m) was significantly larger than that sampled at the top of the sampling mast (0.85 m) (Fig. 5). This finding was confirmed by the good fit (average R^2 0.99) of the exponential functions to the data for calculation of the vertically integrated sediment mass fluxes (Table S1).

The largest horizontal mass flux occurred during the summer months between July and September 2013 at Sites 1, 2, 3 and 5 (Fig. 5). Measurements during this period may have been affected to some degree by rain splash contributing sediment to the lower

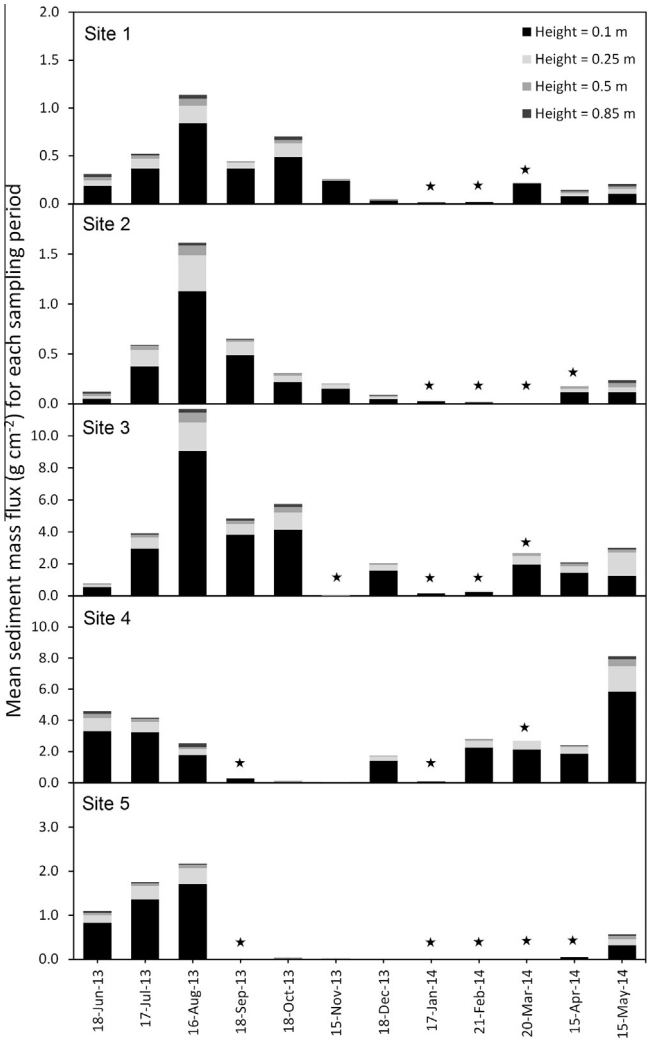

Fig. 5. Horizontal sediment mass flux (g cm^{-2}) for each MWAC sample collection period between 18 May, 2013 and 15 May, 2014. Sample collection dates are shown on the *x*-axis. Sample weights normalized by the MWAC sampler inlet area (0.4715 cm^2) are shown on the *y*-axis. Bars within each column represent sediment collected at four heights (0.1, 0.25, 0.5 and 0.85 m) above ground level. Stars indicate months when data were collected from only one MWAC mast due to blocking of the sampler inlet tubes by insects.

samplers. Horizontal mass fluxes increased in spring 2014 above that recorded during the winter months. With the exception of Site 4, horizontal mass flux did not follow the same seasonal cycle as

Table 4
Summary of threshold wind speed measurements (m s^{-1}) for all sites and seasonal measurements for individual sites over the period 18 May 2013 to 15 May 2014. Records marked with "-" indicate fewer than five transport events occurred for which threshold could be measured.

Location	*n*	Threshold wind speed, U_t (m s^{-1}) at 2.4 m above ground level					
		Min	Quantiles			Mean	Max
			25%	Median	75%		
Site 1	478	3.41	5.35	6.31	7.49	6.56	14.04
Site 2	486	3.44	5.61	7.21	8.77	7.47	16.44
Site 3	441	3.28	7.15	9.65	11.24	9.23	14.80
Site 4	559	2.31	7.08	7.85	8.56	7.69	10.64
Site 5	664	2.85	5.29	6.57	8.20	7.07	13.94
Site 1							
Spring 2013	-	-	-	-	-	-	-
Summer 2013	18	4.48	5.65	6.32	8.04	6.67	9.34
Autumn 2013	283	3.41	5.04	5.80	6.81	6.06	12.04
Winter 2013	137	3.49	6.16	6.98	8.05	7.07	11.27
Spring 2014	38	5.04	6.89	8.00	9.80	8.33	14.04
Site 2							
Spring 2013	-	-	-	-	-	-	-
Summer 2013	26	3.44	5.25	6.99	8.02	6.99	11.51
Autumn 2013	296	3.48	6.58	7.79	9.18	7.95	15.24
Winter 2013	128	3.53	4.94	5.78	7.47	6.44	13.00
Spring 2014	31	4.78	5.54	6.36	7.80	7.42	16.44
Site 3							
Spring 2013	36	4.69	6.39	7.28	8.61	7.41	10.57
Summer 2013	42	3.29	4.80	5.36	5.88	5.54	9.19
Autumn 2013	82	4.46	6.64	8.70	10.71	8.64	12.90
Winter 2013	83	3.96	7.25	8.40	10.34	8.77	12.86
Spring 2014	198	4.74	9.86	11.02	12.00	10.77	14.80
Site 4							
Spring 2013	130	2.31	6.55	7.15	7.51	6.96	9.10
Summer 2013	41	3.80	5.41	6.44	7.23	6.37	8.67
Autumn 2013	63	3.64	7.75	8.22	8.80	8.12	10.46
Winter 2013	88	5.33	7.42	8.15	8.61	7.99	9.54
Spring 2014	237	2.76	7.46	8.21	8.89	8.09	10.64
Site 5							
Spring 2013	51	4.23	6.13	7.54	8.49	7.48	10.25
Summer 2013	54	2.85	6.94	7.79	8.49	7.47	10.00
Autumn 2013	452	3.34	4.95	5.93	6.83	6.07	13.83
Winter 2013	-	-	-	-	-	-	-
Spring 2014	103	3.46	10.12	11.07	12.06	10.88	13.94

the wind (Fig. 4a). Erosive winds driving mass flux at the study sites were generated more often by short-lived convective storm activity and associated cool air outflows during the summer (Warner, 2009), as found by Bergametti and Gillette (2010).

3.4. Threshold dynamics

Significant variability was recorded in U_t at study sites, covering the range ~5–16 m s^{-1} (Table 4). While the variability in U_t was large, the range was similar for each of the sites and the magnitudes of both the mean and median U_t among sites were similar (Table 4). On the basis of the large differences in their soil surface conditions, we expected to have found more pronounced differences in the mean and median wind speed threshold for the different soils. Both the annual mean and median U_t for all sites were within the range 6.31–9.65 m s^{-1} (2.4 m above ground level). Calculated from the minimum and maximum monthly mean z_0 for each site, this translates to approximate mean threshold shear velocity (u_{*t}) values of 0.52–0.56 m s^{-1} for Site 1, 0.48–0.54 m s^{-1} for Site 2, 0.57–0.65 m s^{-1} for Site 3, and 0.59–0.74 m s^{-1} for Site 5. Sites 1, 2, 3 and 5 had multi-modal distributions of U_t for the study period, while Site 4 had a tightly constrained unimodal U_t distribution (Fig. 6). The largest maximum U_t was recorded at Site 2 (16.44 m s^{-1}), while the smallest maximum U_t was recorded at Site 4 (10.64 m s^{-1}). Sites 1, 2 and 5 had a similar annual range and similar probability distributions of U_t, while Site 3 had strong multimodality with U_t modes at 7.25 and 10.96 m s^{-1} (Fig. 6).

No consistent seasonal pattern in U_t was evident in the data. Seasonal differences in U_t among the study sites were pronounced at Sites 3 and 5, but at Sites 1, 2 and 4 seasonal variations in the wind speed threshold were more tightly constrained (Fig. 6). We found that the wind speed threshold in summer 2013 extended to a range of U_t that was smaller than measured in the other seasons, while U_t in spring 2014 was larger than in other seasons at Sites 1, 3 and 5 (Table 4). The occurrence of smaller U_t during summer 2013 may have facilitated the larger measured horizontal mass fluxes at Site 3 at that time, but does not appear to explain the large summertime horizontal mass flux at the other sites (Fig. 5). Similar patterns are evident for the other sites, for which reductions in U_t and increases in wind speed did not always result in increased sediment transport.

The significance of the variability in U_t among sites and between seasons can be evaluated qualitatively in the context of probability distributions of wind speed at the sites. Such analysis must recognize the non-linear mass flux response to U_t (Barchyn and Hugenholtz, 2011), and that the magnitude of mass flux can vary significantly (often by an order of magnitude) even for homogeneous surfaces. This analysis must also recognize the potential effects of differences in the aerodynamic roughness of the fetch outside the cleared study exclosures (Section 3.2). Table 5 reports the probability of wind speed measured at 2.4 m height exceeding a specific value in the range 5–11 m s^{-1}, coincident with the range of most frequently measured U_t. The probabilities of exceeding each wind speed vary among the sites, suggesting that a change in U_t may have slightly different significance for sediment flux depending on location. The consistent pattern of decreasing probabilities for increasing wind speed indicates that the general nature of the sediment flux response to changing U_t may be consistent among sites. However, the large variability in the measured horizontal mass fluxes (Table 3) appears inconsistent with the relatively small differences among sites in both the occurrence of erosive winds (Table 5), and in U_t (Table 3). Similar mass fluxes would have been expected if the erosion process at the sites was only transport limited. Given the large differences in mass flux among the sites, we interpret our results as suggesting that wind energy and the wind speed threshold were not dominant controls on the variability in horizontal mass flux.

4. Discussion and conclusions

The difference between wind shear velocity and the entrainment shear velocity threshold is represented as the dominant control on horizontal mass flux in aeolian sediment transport models (Darmenova et al., 2009; Kok et al., 2014). The significance of the entrainment threshold as a control on the magnitude of the mass flux reflects theory derived for the ideal case of equilibrium saltation, in which the entrainment threshold represents the main land surface control on sediment transport (Bagnold, 1941; Owen, 1964; Creyssels et al., 2009; Kok and Renno, 2009). Field and wind tunnel measurements in a range of agricultural and dryland settings have been evaluated in this context (e.g., Gillette et al., 1980; Gillette, 1988). However, interpretation of the role of the entrainment threshold, and of threshold dynamics, is both location-specific and dependent on how threshold is defined (Webb and Strong, 2011). Our results suggest that for undisturbed dryland soils the entrainment threshold may not always play a dominant role in determining the magnitude of horizontal mass flux.

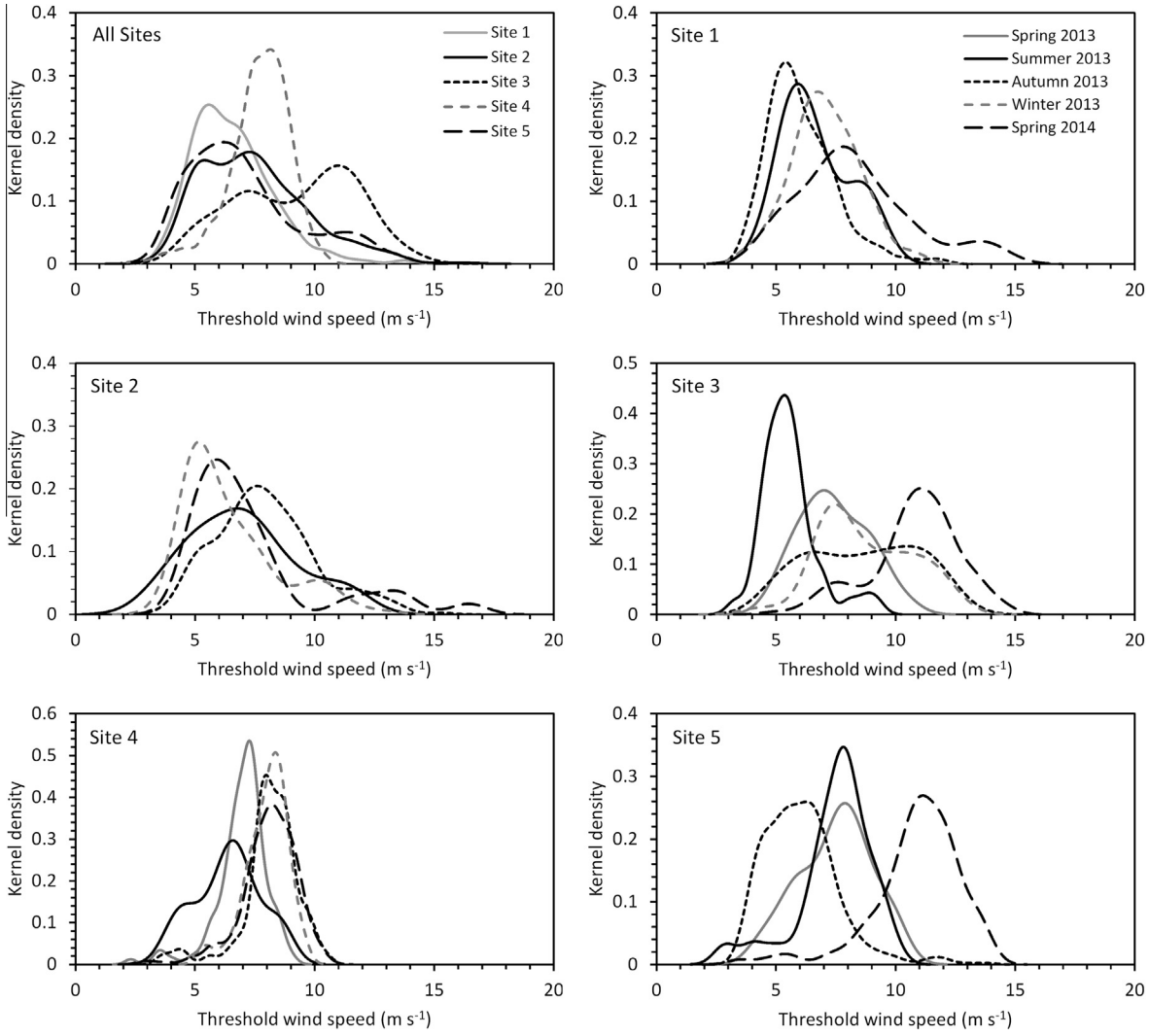

Fig. 6. Kernel density estimates of threshold wind speed (m s^{-1}) for the five study sites. Threshold estimates were obtained using the instantaneous threshold method with a minimum number of particle counts for threshold identification set to 10 counts per minute. Measurement interval: 1 min; sampling interval: 1 Hz; transport measurements: Wenglor YH03PCT08, 0.05 m height; wind measurement: RM Young 3101, 2.4 m height.

Table 5
Probabilities of exceeding measured wind speeds (U) for the range of threshold wind speeds (U_t) at each study site.

Location	Wind speed (U) probabilities (measured at 2.4 m a.g.l)						
	5 m s^{-1}	6 m s^{-1}	7 m s^{-1}	8 m s^{-1}	9 m s^{-1}	10 m s^{-1}	11 m s^{-1}
Site 1	0.086	0.058	0.037	0.022	0.011	0.005	0.002
Site 2	0.074	0.056	0.040	0.027	0.017	0.009	0.005
Site 3	0.069	0.049	0.034	0.021	0.012	0.006	0.003
Site 4	0.053	0.033	0.017	0.007	0.003	0.001	0.001
Site 5	0.057	0.038	0.025	0.015	0.008	0.003	0.001

Differences in the entrainment threshold of soils can be explained by the factors that control soil mobilization by wind (Shao, 2008). At the scale of the soil grain or aggregate, U_t is a function of the grain size, grain density, the strength of cohesive bonds between grains, soil roughness, and atmospheric conditions that influence the air density and inter-particle bonding (Shao and Lu, 2000; Ravi et al., 2006). Changes in the soil moisture content in response to precipitation (rainfall or snowfall) can significantly modify the threshold (Fécan et al., 1999; Sankey et al., 2009; Barchyn and Hugenholtz, 2012). Similarly, the presence of physical and biological soil crusts is often considered to increase the strength of inter-particle bonds, and therefore increase the entrainment threshold (Nickling and Ecclestone, 1981; Nickling, 1984; Belnap and Gillette, 1997; O'Brien and McKenna Neuman, 2012).

On the basis of the highly variable soil surface conditions among our study sites (Table 1), this summary of the controls on the entrainment threshold suggests that we should have found large differences in U_t among the sites, and potentially large differences in U_t between seasons. Large variability in the entrainment threshold have been reported from field and wind tunnel studies of both cropland and rangeland soils (e.g., Gillette et al., 1980; Gillette, 1988; Stout and Arimoto, 2010; Barchyn and Hugenholtz, 2012). However, the small variability in the mean and median U_t among

our sites for the study period indicates that the presence, characteristics (type, strength) and changes in soil crusting may not have had a large effect on the wind speed threshold. Soil crusting appears to have influenced the sediment supply and the soil capacity to release additional sediment into the saltation load when subject to saltation bombardment (Rice et al., 1999; Macpherson et al., 2008).

While the rainfall at our study sites was strongly seasonal, we suspect that high air temperatures (mean maximum > 30 °C from May to September) and evaporative demand (mean pan evaporation 260 mm month^{-1}) significantly reduced soil moisture and humidity effects on U_t in the study area (Wainright, 2006). We interpret the measured seasonal variations in wind speed threshold as being influenced more by changes in the amount and size distribution of loose erodible material at the soil surface in response to the rainfall events and sediment transport by wind, with changes in grain sizes directly affecting the energy required for mobilization by wind (Zobeck and Popham, 1992; Gillette and Chen, 2001). This could explain why U_t did not exhibit a consistent pattern of seasonal variability among the sites, as would be expected if climatic influences had induced significant seasonal changes in the soil cohesion.

If U_t is controlled by the amount and size distribution of loose erodible material on the soil surface, then what other factors contributed to the large variability in horizontal mass flux? A number of factors are known to influence horizontal mass flux. These include atmospheric conditions (Martin et al., 2013), properties of the soil surface (e.g., roughness, moisture content), and feedbacks resulting from interactions between the saltation load, wind velocity profile and the bed that moderate fluid and particle dynamics (Sherman and Farrell, 2008; Creyssels et al., 2009; Charru et al., 2013). Our field data are insufficient to resolve many of these processes, but highlight the need to consider further two additional factors controlling horizontal mass flux. These are (1) the supply of loose erodible material at the sites which could be mobilized as initial saltators (Gillette and Chen, 2001), and (2) differences in the efficiency of saltators to entrain sediment (abrasion efficiency), as determined by saltator impact energy and soil surface hardness and resistance (cohesion) (Rice and McEwan, 2001). While these factors have for a long time been recognized as important controls (Bagnold, 1941), little remains known about their importance, relative to the entrainment threshold, in controlling mass flux.

For example, Sites 1 and 2 produced the smallest horizontal mass fluxes (Table 3). These sites had moderately hard physical crusts and fine textured soils, with smaller sand content and a larger portion of clay aggregates than the other sites (Table 1). These sites also initially had small (<4%) cover of loose erodible material on the soil surface. The combination of the few available saltators and hard surface crusts likely resulted in the small horizontal mass flux for these sites. While having similar U_t to Sites 1 and 2, Sites 4 and 5 had weak surface crusts, initially large (>40%) cover of available quartz saltators (Table 1), and produced larger horizontal mass fluxes (Table 3). The slightly finer soil texture, larger soil $CaCO_3$ content (promoting lower soil cohesion) (Chepil, 1954) and lower amount and height of surrounding vegetation outside the cleared study exclosure at Site 4 were likely responsible for the larger horizontal mass flux at that site relative to Site 5.

Although Site 3 had a relatively hard surface crust and small fraction of *in situ* saltators (Table 1), this site produced the largest horizontal mass fluxes. These results suggest that saltator supply and abrasion efficiency played an important role in determining the magnitude of the mass flux (Rice et al., 1999), which exceeded that of the coarser textured soils with weak crusts and large *in situ* supply of loose erodible material (Sites 4 and 5). The saltators at Site 3 may be more efficient at releasing crusted surface material into the saltation load than those at Sites 1 and 2, which had a similar surface cover of loose erodible material but generated smaller sediment fluxes (Table 3). The large $CaCO_3$ content of the Site 3 soil (Table 1) may also have made the surface more susceptible to abrasion than the other sites (Chepil, 1954). This is an interesting contrast to the soils at Sites 4 and 5, which would typically be regarded as being the most erodible, and despite our results also showing the wind speed thresholds for these sites were often similar (Table 4). We note that under some conditions hard soil surfaces may promote saltation by increasing saltator rebound energies and particle velocities (e.g., McKenna Neuman and Scott, 1998; Ho et al., 2011; Nield and Wiggs, 2011; Rotnicka, 2013). However, our data do not provide direct evidence for separating this factor as a major control on sediment mass flux at the study sites.

Observations at Site 3 suggest that the availability of saltators that can abrade the crusted surface was supplemented by sand grains transported onto the site from adjacent sand ridges during high precipitation and wind events in summer 2013. This off-site contribution of saltators appears to be very important for aeolian sediment transport to occur at this site. Similar processes have been documented in other dust source regions (Bullard and McTainsh, 2003) and the finding illustrates the need to consider landscape setting as a factor influencing the sediment mass flux (Gillette, 1999). A change in the amount and size distribution of saltators for transport at Site 3 with the addition of this material may have resulted in the decline in U_t during summer 2013 (Fig. 6), and contributed to the significantly larger horizontal mass fluxes measured at that time. Further research is needed to quantitatively test these hypotheses in the context of saltation mechanics. This will inevitably require high spatial and temporal resolution measurements in order to parse the mechanics as influenced by the various controls.

Fig. 7 summarizes the factors controlling soil erodibility dynamics, as represented by the sediment emission potential. The entrainment threshold (represented by u_{*_t} or U_t) is one of three main controls on the horizontal mass flux, and generally responsible for determining the initiation of transport, rather than the transport magnitude. In many landscapes the entrainment threshold can be important for the magnitude of the horizontal sediment mass flux (Leys and Raupach, 1991). However, this importance will vary for different systems. At locations where soil crusting is weak or absent and seasonal climate variability has a strong effect on the soil cohesion, e.g., through the soil moisture content, the entrainment threshold can counter the wind transport potential and thus control the frequency and magnitude of sediment flux (e.g., Cornelis and Gabriels, 2003). In sediment supply-limited systems where the soil moisture content is frequently low the entrainment threshold may play a secondary role, relative to saltator supply and abrasion efficiency, in determining the magnitude of the sediment mass flux (O'Brien and McKenna Neuman, 2012). The disturbance of physical and biological soil crusts, for example by livestock trampling or tillage, can increase the erodible sediment supply (Baddock et al., 2011), but may also influence the entrainment threshold by modifying the size distribution of soil grains at the surface (Belnap et al., 2007).

Our results suggest that determining the entrainment threshold as a function of the amount and particle size distribution of loose erodible material at the soil surface may improve estimates of the shear velocity threshold. This approach may also reduce the gap between model estimates and field measurements of U_t and u_{*_t}, which generally do not discriminate particle size (Barchyn and Hugenholtz, 2011). As all of our study sites had some fraction of material that was entrained at approximately similar threshold wind speeds, the application of current equations that predict u_{*_t} as a product of the soil particle size distribution (e.g., Shao and

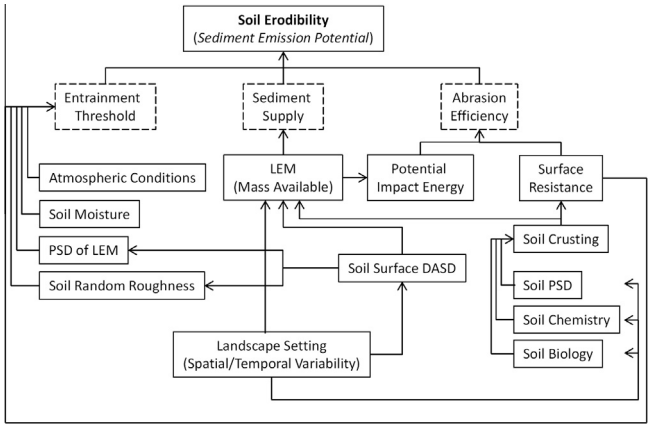

Fig. 7. Conceptual summary of the controls on soil erodibility, defined here as the sediment emission potential for a soil. For simplicity we keep separate the effects of non-erodible roughness elements (e.g., vegetation), which may be considered to affect the landscape erodibility (Webb and Strong, 2011). Acronyms are defined as: particle size distribution (PSD) and loose erodible material (LEM), the erodible fraction (<0.85 mm) of soil grains or aggregates sitting on the soil surface (characterized by the dry aggregate size distribution; DASD). Here, atmospheric conditions include air temperature and humidity (Ravi et al., 2006). The LEM type includes morphology (grain or aggregate), mineralogy and density. The soil chemistry includes the soil salt, organic carbon and $CaCO_3$ contents, while soil biology refers to the presence of crust-forming biota such as cyanobacteria, lichens and fungi (Belnap, 2003). Together these determine the potential impact energy of the saltators and the energy required to release sediment from the surface (surface resistance) (Rice et al., 1999). Landscape setting determines the nature of spatial and temporal variations in soil properties and geomorphic processes that may influence sediment supply and the entrainment threshold. Weather, climate and disturbance are expected to interact with landscape setting to influence all of the land surface conditions at different spatial and temporal scales (Webb and Strong, 2011).

Lu, 2000) may well continue to provide a reliable first approximation of the entrainment threshold.

Reliably estimating sediment supply and bed resistance to abrasion, and representing their effects on the saltation load, are possibly the greatest challenges that need to be addressed for the development of a generalizable horizontal mass flux scheme. Cropland wind erosion models, such as the Revised Wind Erosion Equation (Fryrear et al., 1998) and Wind Erosion Prediction System (Hagen, 1991), represent the effects of soil crusting and loose erodible material (through the aggregate size distribution) on sediment mass flux. However, very few studies have attempted to relate environmental and surface conditions to the amount of crusting and loose erodible material (Zobeck and Popham, 1992). While applying these models for regional and global applications is non-trivial, they provide insights to how horizontal mass flux can be represented when Owen's second hypothesis does not hold (Owen, 1964). Exploring further the intensity and duration of saltation with respect to the entrainment threshold and wind speed may provide further insights to the processes that will facilitate scheme development. Conducting this research for a range of dryland and agricultural settings may also provide generality in our process understanding that has arguably not been included in existing horizontal mass flux equations. Proximal remote sensing approaches have potential to provide additional information on changes in soil surface conditions that moderate the sediment mass flux (Chappell et al., 2006). Evaluating quantitatively these relationships and the interactive effects of static and dynamic soil properties is the subject of ongoing research at the study sites.

Finally, our research has highlighted again the need for a new horizontal mass flux scheme that enables estimation of the sediment mass flux under both transport-limited and supply-limited conditions. Such a scheme would represent the initiation of horizontal mass flux at the entrainment threshold and then estimate the sediment flux as a function of wind shear velocity, the mass of available saltators at the soil surface and the release of sediment into the saltation load due to saltation bombardment and abrasion. In a broader context, models would also ideally account for landscape setting and connectivity (Okin et al., 2009), which influence the availability of upwind saltator material. While our study was not designed to quantitatively address these sources of variability, our observations suggest that they have significant explanatory power, particularly in heterogeneous landscapes. The geomorphic patterns in the Jornada Basin are typical of those in many dryland regions where aeolian and fluvial processes create mosaics of fine- and coarse-texture land surfaces at multiple spatial scales. As a start, capturing supply limitation and saltation bombardment processes would provide greater continuity in the representation of horizontal and vertical mass fluxes, and may help to reduce the large uncertainty in aeolian sediment transport predictions.

Acknowledgments

This research was supported by funding from the Department of Interior, Bureau of Land Management. We thank Lauren Svejcar for assistance with site establishment and soil and vegetation surveys, Brad Cooper for sample collection and servicing the field sites, Dean Holder for assistance with the soil analyses, and the anonymous reviews for constructive comments on the manuscript. Any use of trade, product, or firm names is for descriptive purposes only and does not imply endorsement by the U.S. Government. The USDA is an equal opportunity provider and employer.

Appendix A. Supplementary data

Supplementary data associated with this article can be found, in the online version, at http://dx.doi.org/10.1016/j.aeolia.2015.11.006.

References

Baddock, M.C., Zobeck, T.M., Van Pelt, R.S., Fredrickson, E.L., 2011. Dust emissions from undisturbed and disturbed, crusted playa surfaces: cattle trampling effects. Aeol. Res. 3, 31–41.
Bagnold, R.A., 1937. The transport of sand by wind. Geogr. J. 89, 409–438.
Bagnold, R.A., 1941. The Physics of Blown Sand and Desert Dunes. Methuen, London.
Barchyn, T.E., Hugenholtz, C.H., 2011. Comparison of four methods to calculate aeolian sediment transport threshold from field data: implications for transport prediction and discussion of method evolution. Geomorphology 129, 190–203.
Barchyn, T.E., Hugenholtz, C.H., 2012. Winter variability of aeolian sediment transport threshold on a cold-climate dune. Geomorphology 177, 38–50.
Barchyn, T.E., Hugenholtz, C.H., Li, B., McKenna Neuman, C., Sanderson, S., 2014. From particle counts to flux: wind tunnel testing and calibration of the 'Wenglor' aeolian sediment transport sensor. Aeol. Res. 15, 311–318.
Belnap, J., 2003. Biological crusts and wind erosion. In: Belnap, J., Lange, L. (Eds.), Biological Soil Crusts: Structure, Function, and Management, Ecological Studies: Analysis and Synthesis 150. Springer-Verlag, Berlin, pp. 339–347.
Belnap, J., Gillette, D.A., 1997. Disturbance of biological soil crusts: impacts on potential wind erodibility of sandy desert soils in southeastern Utah. Land Degrad. Dev. 8, 355–362.
Belnap, J., Phillips, S.L., Herrick, J.E., Johansen, J.R., 2007. Wind erodibility of soils at Fort Irwin, California (Mojave Desert), USA, before and after trampling disturbance: implications for land management. Earth Surf. Proc. Land. 32, 75–84.
Bergametti, G., Gillette, D.A., 2010. Aeolian sediment fluxes measured over various plant/soil complexes in the Chihuahuan desert. J. Geophys. Res. 115 (F03044), 2010. http://dx.doi.org/10.1029/2009JF001543.
Bullard, J.E., McTainsh, G.H., 2003. Aeolian–fluvial interactions in dryland environments: examples, concepts and Australia case study. Prog. Phys. Geogr. 27, 279–310.
Chappell, A., Zobeck, T.M., Brunner, G., 2006. Using bi-directional soil spectral reflectance to model soil surface changes induced by rainfall and wind-tunnel abrasion. Remote Sens. Environ. 102, 328–343.

Chappell, A., Warren, A., O'Donoghue, A., Robinson, A., Thomas, A., Bristow, C., 2008. The implications for dust emission modeling of spatial and vertical variations in horizontal dust flux and particle size in the Bodélé Depression, Northern Chad. J. Geophys. Res. 113 (D04214), 2008. http://dx.doi.org/10.1029/2007JD009032.
Charru, F., Andreotti, B., Claudin, P., 2013. Sand ripples and dunes. Annu. Rev. Fluid Mech. 45, 469–493.
Chepil, W.S., 1954. Factors that influence clod structure and erodibility of soil by wind. III. Calcium carbonate and decomposed organic matter. Soil Sci. 77, 473–480.
Cornelis, W.M., Gabriels, D., 2003. The effect of surface moisture on the entrainment of dune sand by wind: an evaluation of selected models. Sedimentology 50, 771–790.
Creyssels, M., Dupont, P., Ould el-Moctar, A., Valance, A., Cantat, I., Jenkins, J.T., Pasini, J.-M., Rasmussen, K.R., 2009. Saltating particles in a turbulent boundary layer: experiment and theory. J. Fluid Mech. 625, 47–74.
Darmenova, K., Sokolik, I.N., Shao, Y., Marticorena, B., Bergametti, G., 2009. Development of a physically based dust emission module within the Weather Research and Forecasting (WRF) model: assessment of dust emission parameterizations and input parameters for source regions in Central and East Asia. J. Geophys. Res. 114 (D14201), 2009. http://dx.doi.org/10.1029/2008JD011236.
Duran, O., Claudin, P., Andreotti, B., 2011. On aeolian transport: grain–scale interactions, dynamical mechanisms and scaling laws. Aeol. Res. 3, 243–270.
Duran, O., Andreotti, B., Claudin, P., 2012. Numerical simulation of turbulent sediment transport, from bed load to saltation. Phys. Fluids 24, 103306.
Fécan, F., Marticorena, B., Bergametti, G., 1999. Parameterization of the increase of the aeolian erosion threshold wind friction velocity due to soil moisture for arid and semi-arid areas. Ann. Geophys. 17, 149–157.
Floyd, K.W., Gill, T.E., 2011. The association of land cover with aeolian sediment production at Jornada Basin, New Mexico, USA. Aeol. Res. 3, 55–66.
Fryrear, D.W., Saleh, A., Bilbro, J.D., 1998. A single event wind erosion model. Trans. ASAE 41, 1369–1374.
Gillette, D.A., 1988. Threshold friction velocities for dust production for agricultural soils. J. Geophys. Res. 93 (D10), 12645–612622.
Gillette, D.A., 1999. A qualitative geophysical explanation for "Hot Spot" dust emitting source regions. Contrib. Atmos. Phys. 72, 67–77.
Gillette, D.A., Chen, W., 2001. Particle production and aeolian transport from a "supply-limited" source area in the Chihuahuan desert, New Mexico, United States. J. Geophys. Res. 106 (D6), 5267–5278.
Gillette, D.A., Adams, J., Endo, A., Smith, D., Kihl, R., 1980. Threshold velocities for input of soil particles into the air by desert soils. J. Geophys. Res. 85, 5621–5630.
Gillette, D.A., Herrick, J.E., Herbert, G., 2006. Wind characteristics of mesquite streets in the northern Chihuahuan Desert, New Mexico, USA. Environ. Fluid Mech. 6, 241–275.
Gillies, J.A., Nield, J.M., Nickling, W.G., 2014. Wind speed and sediment transport recovery in the lee of a vegetated and denuded nebkha within a nebkha dune field. Aeol. Res. 12, 135–141.
Goossens, D., Offer, Z.Y., London, G., 2000. Wind tunnel and field calibration of five aeolian sand traps. Geomorphology 35, 233–252.
Hagen, L.J., 1991. A wind erosion prediction system to meet user needs. J. Soil Water Conserv. 46, 106–111.
Herrick, J.E., Van Zee, J.W., Havstad, K.M., Burkett, L.M., Whitford, W.G., 2005. Monitoring Manual for Grassland, Shrubland and Savanna Ecosystems. Volume I. Quick Start. USDA-ARS Jornada Experimental Range, Las Cruces, New Mexico, USA.
Ho, T.D., Valance, A., Dupont, P., Ould El Moctar, A., 2011. Scaling laws in aeolian sand transport. Phys. Rev. Lett. 106, 094501.
Jenkins, J.T., Valance, A., 2014. Periodic trajectories in Aeolian sand transport. Phys. Fluids Am. Inst. Phys. (AIP) 2014, 073301.
Kawamura, R., 1951. Study of sand movement by wind. In: Hydraulic Engineering Laboratory Report HEL-2-8. University of California, Berkeley, USA, p. 57.
Kok, J.R., Renno, N.O., 2009. A comprehensive numerical model of steady state saltation (COMSALT). J. Geophys. Res. 114 (D17204), 2009. http://dx.doi.org/10.1029/2009JD011702.
Kok, J.F., Mahowald, N.M., Fratini, G., Gillies, J.A., Ishizuka, M., Leys, J.F., Mikami, M., Park, M.-S., Park, S.-U., Van Pelt, R.S., Zobeck, T.M., 2014. An improved dust emission model. Part 1: model description and comparison against measurements. Atmos. Chem. Phys. 14, 13023–13041.
Lettau, K., Lettau, H.H., 1978. Experimental and micro-meteorological field studies of dune migration. In: Lettau, H.H., Lettau, K. (Eds.), Exploring the World's Driest Climate, IES Report, 101. University of Wisconsin-Madison, Institute for Environmental Studies, Madison, Wisconsin, USA, pp. 110–147.
Leys, J.F., Raupach, M.R., 1991. Soil flux measurements using a portable wind tunnel. Aust. J. Soil Res. 29, 533–552.
Macpherson, T., Nickling, W.G., Gillies, J.A., Etymezian, V., 2008. Dust emissions from undisturbed and disturbed supply-limited desert surfaces. J. Geophys. Res. 113, F02S04. http://dx.doi.org/10.1029/2007JF000800, 002008.
Marticorena, B., Kardous, M., Bergametti, G., Callot, Y., Chazette, P., Khatteli, H., Le Hegarat-Mascle, S., Maille, M., Rajot, J.-L., Vidal-Madjar, D., Zribi, M., 2006. Surface and aerodynamic roughness in arid and semiarid areas and their relation to radar backscatter coefficient. J. Geophys. Res. 111, F03017. http://dx.doi.org/10.1029/2006JF00046.
Martin, R.L., Barchyn, T.E., Hugenholtz, C.H., Jerolmack, D.J., 2013. Timescale dependence of aeolian sand flux observations under atmospheric turbulence. J. Geophys. Res.: Atmos. 118, 9078–9092.
Massey, J.C., 2013. A Wind Tunnel Investigation to Examine the Role of Air Humidity in Controlling the Threshold Shear Velocity of a Surface and in Controlling the Mass Flux of Material from a Surface (M.S. thesis). Texas Tech University, 59 pp.
McClaran, M.P., Van Devender, T.R., 1997. The Desert Grassland. University of Arizona Press, Tucson, Arizona, USA.
McKenna Neuman, C., Scott, M.M., 1998. A wind tunnel study of the influence of pore water on aeolian sediment transport. J. Arid Environ. 39, 403–419.
Monger, H.C., 2006. Soils development in the Jornada basin, in structure and function of a Chihuahuan Desert ecosystem. In: Havstad, K.M., Huenneke, L.F., Schlesinger, W.H. (Eds.), The Jornada Basin Long-Term Ecological Research Site. Oxford University Press, New York, USA, pp. 81–106.
Namikas, S.L., Sherman, D.J., 1995. A review of the effects of surface moisture content on aeolian sand transport. In: Tchakerian, V.P. (Ed.), Desert Aeolian Processes. Chapman and Hall, New York, pp. 269–293.
Nickling, W.G., 1984. The stabilizing role of bonding agents on the entrainment of sediment by wind. Sedimentology 31, 111–117.
Nickling, W.G., Ecclestone, M., 1981. The effects of soluble salts on the threshold shear velocity of fine sand. Sedimentology 28, 505–510.
Nield, J.M., Wiggs, G.F.S., 2011. The application of terrestrial laser scanning to aeolian saltation cloud measurement and its response to changing surface moisture. Earth Surf. Proc. Land. 36, 273–278.
O'Brien, P., McKenna Neuman, C., 2012. A wind tunnel study of particle kinematics during crust rupture and erosion. Geomorphology 174, 149–160.
Okin, G.S., Parsons, A.J., Wainwright, J., Herrick, J.E., Bestelmeyer, B.T., Peters, D.C., Fredrickson, E.L., 2009. Do changes in connectivity explain desertification? Bioscience 59, 237–244.
Owen, P.R., 1964. Saltation of uniform grains in air. J. Fluid Mech. 20, 225–242.
Ravi, S., Zobeck, T.M., Over, T.M., Okin, G.S., D'Odorico, P., 2006. On the effect of moisture bonding forces in air-dry soils on threshold friction velocity of wind erosion. Sedimentology 53, 597–609.
Rice, M.A., McEwan, I.K., 2001. Crust strength: a wind tunnel study of the effect of impact by saltating particles on cohesive soil surfaces. Earth Surf. Proc. Land. 26, 721–733.
Rice, M.A., McEwan, I.K., Mullins, C.E., 1999. A conceptual model of wind erosion of soil surfaces by saltating particles. Earth Surf. Proc. Land. 24, 383–392.
Rotnicka, J., 2013. Aeolian vertical mass flux profiles above dry and moist sandy beach surfaces. Geomorphology 187, 27–37.
Sankey, J.B., Germino, M.J., Glenn, N.F., 2009. Relationships of post-fire aeolian transport to soil and atmospheric conditions. Aeol. Res. 1, 75–85.
Shao, Y., 2008. Physics and Modelling of Wind Erosion. Kluwer Academic Publishers, London.
Shao, Y., Lu, H., 2000. A simple expression for wind erosion threshold friction velocity. J. Geophys. Res. 105 (D17), 22437–422443.
Shao, Y., Raupach, M.R., Findlater, P.A., 1993. Effect of saltation bombardment on the entrainment of dust by wind. J. Geophys. Res. 98 (D7), 12719–12726.
Shao, Y., Ishizuka, M., Mikami, M., Leys, J.F., 2011. Parameterisation of size-resolved dust emission and validation with measurements. J. Geophys. Res. 116 (D08203), 2011. http://dx.doi.org/10.1029/2010JD014527.
Sherman, D.J., 1992. An equilibrium relationship for shear velocity and roughness length in aeolian saltation. Geomorphology 5, 419–431.
Sherman, D.J., Farrell, E.J., 2008. Aerodynamic roughness lengths over movable beds: comparison of wind tunnel and field data. J. Geophys. Res.: Earth Surf. 113, F02S08. http://dx.doi.org/10.1029/2007JF000784.
Sherman, D.J., Li, B., 2012. Predicting aeolian sand transport rates: a reevaluation of models. Aeol. Res. 3, 371–378.
Sherman, D.J., Li, B., Ellis, J.T., Farrell, E.J., Maia, L.P., Granja, H., 2013. Recalibrating aeolian sand transport models. Earth Surf. Proc. Land. 38, 169–178.
Soil Survey Division Staff, 1993. Soil survey manual. Soil Conservation Service, U.S. Department of Agriculture Handbook 18, Washington, D.C.
Stout, J.E., Arimoto, R., 2010. Threshold wind velocities for sand movement in the Mescalero Sands of southeastern New Mexico. J. Arid Environ. 74, 1456–1460.
Thomson, M., 2006. Representing Data Distributions with Kernel Density Estimates AMCTB No. 4. Analytical Methods Committee, Royal Society of Chemistry, Cambridge, UK.
Wagner, S.W., Hanson, J.D., Olness, A., Voorhees, W.B., 1998. A volumetric inorganic carbon analysis system. Soil Sci. Soc. Am. J. 62, 690–693.
Wainright, J., 2006. Climate and climatological variations in the Jornada Basin. In: Havstad, K.M., Huenneke, L.F., Schlesinger, W.H. (Eds.), Structure and Function of a Chihuahuan Desert Ecosystem: The Jornada Basin Long-Term Ecological Research Site. Oxford University Press, New York, USA, pp. 44–80.
Warner, T.T., 2009. Desert Meteorology. Cambridge University Press, Cambridge.
Webb, N.P., Strong, C.L., 2011. Soil erodibility dynamics and its representation in wind erosion and dust emission models. Aeol. Res. 3, 165–180.
Webb, N.P., Okin, G.S., Brown, S., 2014. The effect of roughness elements on wind erosion: the importance of surface shear stress distribution. J. Geophys. Res.: Atmos. 119, 6066–6084.
Werner, B.T., 1990. A steady-state model of wind-blown sand transport. J. Geol. 98, 1–17.

Wiggs, G.F.S., Livingstone, I., Thomas, D.S.G., Bullard, J.E., 1996. Airflow and roughness characteristics over partially vegetated linear dunes in the southwest Kalahari Desert. Earth Surf. Proc. Land. 21, 19–34.
Wiggs, G.F.S., Baird, A.J., Atherton, R.J., 2004. The dynamic effects of moisture on the entrainment and transport of sand by wind. Geomorphology 59, 13–30.
Zobeck, T.M., 2004. Rapid soil particle size analyses using laser diffraction. Appl. Eng. Agr. 20, 633–639.
Zobeck, T.M., Popham, T.W., 1992. Influence of microrelief, aggregate size and precipitation on soil crust properties. Trans. ASAE 35, 487–492.
Zobeck, T.M., Sterk, G., Funk, R., Rajot, J.L., Stout, J.E., Van Pelt, R.S., 2003. Measurement and data analysis methods for field-scale wind erosion studies and model validation. Earth Surf. Proc. Land. 28, 1163–1188.
Zobeck, T.M., Baddock, M., Van Pelt, R.S., Tatarko, J., Acosta-Martinez, V., 2013. Soil property effects on wind erosion of organic soils. Aeol. Res. 10, 43–51.